Supporting Information

Multifunctional carbon materials from rugosa rose for energy storage and water purification

Peng-Hui Li [a,b] Hui Zhou [c,d] and Wen-Juan Wu [a,b,*]

[a] Jiangsu Co-Innovation Center of Efficient Processing and Utilization of Forest Resources, Nanjing Forestry University, Nanjing, 210037, P.R.China.

[b] College of Light Industry and Food Engineering, Nanjing Forestry University, Nanjing, 210037, P.R.China.

[c] College of Chemical Engineering, East China University of Science and Technology, Shanghai, 200237, P.R. China.

[d] State Key Laboratory of Chemical Engineering, Shanghai, 200237, P.R.China.

1 Material Characterization

1.1 SEM

A field emission scanning electron microscope (Quanta 20, Hitachi, Japan) was used to observe the microscopic morphological characteristics of RRC and NRRC. Before the SEM test, the black powder sample was attached to the conductive adhesive of the sample table and sprayed with gold treatment to eliminate static electricity.

1.2 Raman

The RRC and NRRC were analyzed by Raman spectroscopy using a laser Raman spectrometer (DXR532, Themor, USA) under 532 nm light excitation by taking trace samples on slides.

1.3 XPS

An X-ray photoelectron spectrometer (Ultra DLD, Shimadzu, Japan) was used to determine the surface chemical composition of the samples, including details of the surface elemental composition and C (C 1s), N (N 1s) and O (O 1s) peaks. Samples were detected at concentrations greater than 0.10 % and detection depths less than 10 nm. At least two samples were prepared for each raw material, and at least three different locations were determined for each sample. Include the relative content of elements and the type and relative content of chemical functional groups.

1.4 XRD

The crystal structure analysis of RRC and NRRC was performed on a combined multifunctional horizontal X-ray diffractometer (Ultima IV, Nippon Rigaku). Test conditions: X-ray tube with CuKα target (λ = 0.15406 nm), graphite monochromator to eliminate CuKα radiation, tube voltage of 40 kV, tube current of 200 mA, scan range of 2θ = 5 ~ 60°, scan step of 0.02°, scan rate of 15 °/min.

1.5 BET

N_2 (77 K) adsorption/desorption isotherms and textural properties of the RRC and NRRC were obtained by a Micromeritics ASAP-2460 (Micromeritics, USA) surface area and pore size analyzer. The thermostatic adsorption-desorption curves were used to calculate the information of specific surface area, pore volume and pore size distribution of carbon materials. Total pore volume was determined according to the single point method at a relative pressure (P/P_0) of 0.998.

Table S1 BET results for RRC and NRRC

Sample	S_{BET} [a] (m^2/g)	$V_{Total\ pore}$ [b] (cm^3/g)	$V_{Micropore}$ [c] (cm^3/g)	Daver [d] (nm)
RRC	1019	0.52	0.45	2.79
NRRC	1393	0.68	0.61	2.71

[a] Total surface area calculated by the BET method.

[b] Total pore volume calculated at $P/P_0 = 0.99$.

[c] Micropore volume calculated from t-plot method.

[d] Average pore diameter calculated from BJH desorption.

1.6 TEM

The specimen was crushed and dispersed in ethanol. The resulting suspension was scooped onto a copper grids covered with holey carbon film; then the specimen was dried under magnesium lamp. SAED patterns and HRTEM images were recorded using a TEM device (Model JEM-2100UHR, JEOL, Tokyo,Japan) at an accelerating voltage of 200 kV.

2 Electrochemical Measurements

2.1 Preparation of electrodes

The RRC or NRRC sample, conductive carbon black and binder (polyvinylidene fluoride) are stirred well in a weight ratio of 8:1:1. 4-5 drops of N-methylpyrrolidone solution was applied uniformly to the pretreated nickel foam with a loading of about 3-5 mg/cm^2 active material per electrode. The mixture was pressed onto the nickel foam at a pressure of 10 MPa and dried under vacuum at 80°C for 12 h to complete the working electrode preparation.

The electrode plates were assembled into symmetrical supercapacitors with electrode shells of CR2032 type and the same material for both positive and negative electrodes, which were carbon materials prepared in this experiment. 6 mol/L KOH aqueous solution was used as electrolyte and two pretreated nickel foams with similar active materials were pressed under 10 MPa pressure selected. Encapsulated in 2032 electrode shells with a sealer and rested for 12 h for electrochemical tests [S1].

2.2 Test performance

To further investigate the feasibility of RRC and NRRC samples as supercapacitor electrode materials, RRC and NRRC samples were assembled into a symmetric liquid double electrode system for CV and GCD tests, respectively. Two equal masses of RRC and NRRC carbon material electrode sheets were assembled into a button-type symmetric supercapacitor in the order of cell

case, positive electrode, diaphragm, negative electrode, and cell case. Three-electrode system: Electrochemical measurements were performed in a 6 M KOH solution with a potential window of -1.0 to -0.2 V. Cyclic voltammetric curves (CV) of the working electrodes were tested in the voltage range from 0 V to 1 V and different scan rates (10, 20, 30, 50, and 100 mV/s) were used to investigate the multiplicity characteristics. Galvanostatic charge/discharge curves (GCD) were examined at current densities (0.5, 1, 2, 4 and 10 A/g) within the voltage range of -1 V to 0 V. Two-electrode system: Electrochemical measurements were performed in a 6 M KOH solution with a potential window of 0 to 1 V. CV of the working electrodes were tested in the voltage range from 0 V to 1 V and different scan rates (10, 20, 30, 50, and 100 mV/s) were used to investigate the multiplicity characteristics. GCD were examined at current densities (0.5, 1, 3, 5, 10 and 20 A/g) within the voltage range of 0 V to 1 V. The specific capacitance of the electrode material can be obtained based on Equation (S2) [S2].

Electrochemical impedance spectroscopy was performed using an electrochemical workstation (CS350M electrochemical workstation, Corrtest, Wuhan, China) for a carbon electrode in the frequency range of 10^{-2}-10^{5} Hz with an amplitude of 5 mV and an initial open circuit voltage. The cycling performance of the carbon material electrodes was evaluated by charging and discharging at a current density of 10 A/g after 10000 cycles.

The linear charge/discharge curve equation is shown in (S1):

$$C_m = C/m = I\Delta t/(m\Delta v) \quad \text{(S1)}$$

where C_m (F/g) is the specific capacitance; m (g) is the electrode material loading; I (A) is the charge/discharge current; Δt (s) is the charge/discharge time; ΔV (V) is the voltage window.

The nonlinear charge/discharge curve equation is shown in (S2).

$$C_m = \frac{2\times I\times S}{m\times \Delta U^2} = \frac{2\times I\int_{t(U_{max})}^{t(U_{min})} U(t)dt}{m\times \Delta U^2} \quad \text{(S2)}$$

where: I (A) is the charge/discharge current; S (Vs) is the integrated area under the discharge curve; m (g) is the active material of the electrode; t (U_{max}) is the time (s) for the start of discharge; t (U_{min}) is the time (s) for the end of discharge; ΔU (V) is the voltage range after deducting the voltage drop.

The energy density and power density are expressed by the following equations (S3)-(S4):

$$E = \frac{CV^2}{2} \quad \text{(S3)}$$

$$P = \frac{E}{t} \quad \text{(S4)}$$

where C (F/g) is the specific capacitance of the supercapacitor, E (Wh/kg) is the energy density of the supercapacitor, V (V) is the operating voltage, P (W/kg) is the power density of the supercapacitor, and t (h) is the discharge time.

3 Adsorption measurement

3.1 Determination of maximum absorption wavelength

The MB was accurately weighed for the corresponding organic pollutants, and a 10 mg/L master dye solution was accurately configured in a volumetric flask. Absorption or reflectance in the visible range directly affects the perceived color of the chemicals involved, and the full spectrum of the two organic pollutant solutions can be scanned by a UV spectrophotometer (UV2200, Shanghai Sunyu Hengping Scientific Instrument Co., Ltd.) to determine the maximum absorption wavelength of the dyes, respectively. The test method was quantitatively measured using UV-Vis, and the corresponding maximum absorption wavelengths of the three dyes, MB, MO, and RhB, were: 665 nm, 464 nm, and 554 nm, respectively.

3.2 Determination of standard curve

Different concentration gradients of MB (1 mg/L, 2 mg/L, 2.5 mg/L, 3 mg/L, 4 mg/L) were prepared, and the absorbance of the corresponding organic pollutant solutions at the maximum absorption wavelength was measured at different concentrations, and the linear relationship between the organic pollutant absorbance and the organic pollutant concentration was fitted by the organic pollutant absorbance and the organic pollutant concentration, and the correlation coefficient, R^2, was used to judge the merit of the fitting relationship (the correlation coefficient was 0.99 or higher). As a result, the standard curve of the organic pollutant solution was obtained, and the basic information of MB organic dyes and the relevant parameters of the fitted standard curve equation were shown in Fig. S1 [S3].

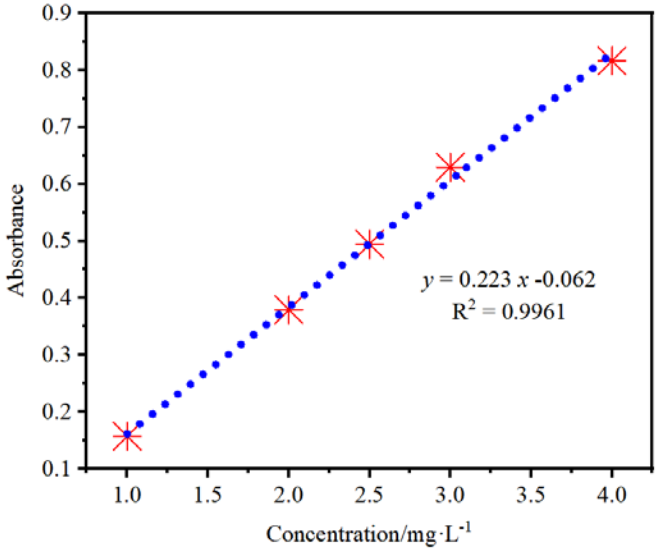

Fig. S1 Methylene blue standard curve

In order to investigate the adsorption performance of the two adsorbents, NRRC and RRC, the single variable method was adopted for different initial concentrations and adsorbent dosages. After adsorption, the supernatant was filtered with 0.22 μm filter membrane, and the removed supernatant was tested for absorbance with UV spectrophotometer, and if the absorbance was too high, it was diluted and then measured for its absorbance. For the effect of adsorbent dosage, the above dried to constant weight NRRC and RRC carbon materials (10 mg, 20 mg, 30 mg, 40 mg) were accurately weighed and placed in 100 ml of dye solution and placed in a thermostatic oscillator at a speed of

150 rpm for 30 min at 25°C. Then, the absorbance of the adsorbed material was measured, and the corresponding adsorption concentration was calculated from the standard curve. Then, the absorbance was measured and the corresponding adsorption concentration was calculated from the standard curve, and the adsorbed amount of dye was calculated according to the following equation S5:

$$q_e = (C_0 - C_e)\mathrm{V/m} \tag{S5}$$

Where, q_e - the adsorption capacity of the adsorbent to the dyes after the adsorption is completed, mg/g;

C_0 - denotes the initial concentration of MG solution, mg/L;

C_e - denotes the concentration of MG solution after adsorption, mg/L;

V, m - volume of dye to be adsorbed, L; mass of adsorbent, g.

3.3 Mechanism analysis of adsorption process

Adsorption kinetics and isotherm modeling were used to illustrate the law and internal mechanism of the adsorption process. Based on the experimental data, the model was fitted and the model parameters were analyzed to investigate the mechanism of the adsorption process of the adsorbent. The equations of the evaluated models are as follows.

Four kinetic models: pseudo-first order, pseudo-second order, Elovich, and intraparticle diffusion model.

Pseudo-first-order kinetic model:

$$\ln（\mathrm{q_e} - \mathrm{q_t}) = \ln \mathrm{q_e} - k_1 t \tag{S6}$$

Pseudo-second-order kinetic model:

$$\frac{t}{\mathrm{q_t}} = \frac{t}{\mathrm{q_e}} + \frac{1}{k_2 \mathrm{q_e}^2} \tag{S7}$$

Intraparticle diffusion kinetic model:

$$\mathrm{q_t} = k_{\mathrm{id}} t^{0.5} + c \tag{S8}$$

Elovich kinetic model:

$$\mathrm{q_t} = \frac{1}{\beta}\ln(\alpha\beta) + \frac{1}{\beta}\ln t \tag{S9}$$

In the above kinetic models, k_1 ($\mathrm{min^{-1}}$) denotes the pseudo-first order adsorption rate constant; k_2 ($\mathrm{g\cdot mg^{-1}\cdot min^{-1}}$) denotes the pseudo-second order adsorption rate constant; k_{id} ($\mathrm{g\cdot mg^{-1}\cdot min^{0.5}}$) denotes the rate constant for the internal diffusion model, and c denotes the intercept; α ($\mathrm{g\cdot mg^{-1}}$) and β ($\mathrm{g\cdot mg^{-1}\cdot min}$) denote the initial Elovich model adsorption and desorption constants for the Elovich model.

Four isotherm models: Langmuir, Freundlich, Temkin, and Dubinin-Radushkevich model.

Langmuir model:

$$\frac{C_e}{q_e} = \frac{C_e}{q_m} + \frac{1}{K_L q_m} \quad \text{(S6)}$$

Freundlich model:

$$\ln q_e = \ln K_F + \frac{1}{n} \ln C_e \quad \text{(S7)}$$

Temkin model:

$$q_e = \frac{RT}{b_t} \ln a_t + \frac{RT}{b_t} \ln C_e \quad \text{(S8)}$$

Dubinin-Radushkevich model:

$$\ln q_e = \ln Q_m - B\varepsilon^2$$

$$\varepsilon^2 = RT \ln\left(1 + \frac{1}{C_e}\right) \quad \text{(S9)}$$

In the above isothermal model, q_m represents the maximum adsorption, q_e and q_t (mg/g) represent the adsorbed amount at adsorption equilibrium and at time t, respectively; K_L and K_F denote the Langmuir and Freundlich constants, respectively; R and T denote the ideal gas constant and the absolute temperature of the adsorption process, respectively, and a_t and b_t both denote the Temkin constants; ε denotes the Polanyi adsorption energy, and B denotes the Dubinin-Radushkevich constant.

3.5 Regeneration of NRRC

After adsorption equilibrium, the NRRC was washed with 250 mL of distilled water to remove the adsorbed dye. The adsorbent was then treated with 60 mL of ethanol and shaken in a constant temperature water bath at a certain temperature. After desorption, the NRRC was rapidly dried in a vertical blast drying oven and later used to study the reusability of NRRC.

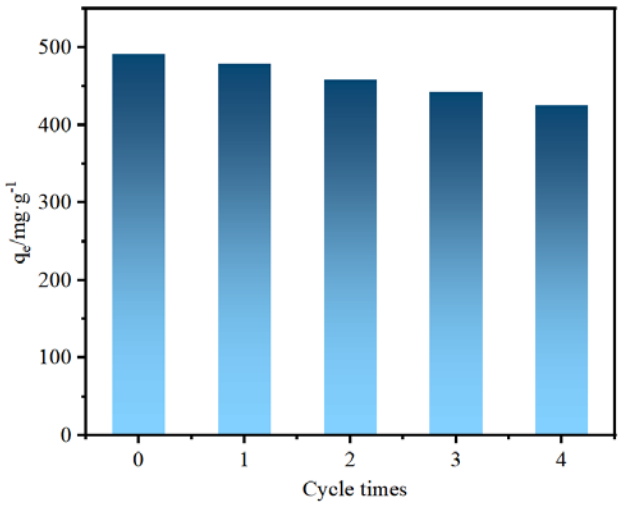

Fig. S2 Adsorption capacity of MB on NRRC four consecutive adsorption-desorption cycles

Note: Experimental conditions (adsorbed dye is MB, dosage 40 mg, pH = 7, dye concentration 200 mg/L, ethanol dose: 60 ml/dose).

Table S2 Specific capacitances of carbon electrodes prepared from biomass evaluated for 6 M KOH electrolyte concentrations.

Carbon materials	Preparation method	S_{BET} (m^2/g)	Current density (A/g)	Specific capacitance (F/g)	Cycling stability	Ref.
Kapok flower	KOH activation	1904	1	287	97% (5000th cycle)	S4
Corncob residue	Steam activation	1210	1	120	82% (100000th cycle)	S5
Fallen leaves	KOH&K_2CO_3 activation	1078	0.5	310	99% (2000th cycle)	S6
Lignosulfonate/graphene	Co-pyrolysis with urea	515	0.2	177	93% (1000th cycle)	S7
Lignin	Hard-template	803	0.1	208	96% (1500th cycle)	S8
Chestnut shell	Melamine activation	692	0.5	403	97% (20000th cycle)	S9
Willow catkins	KOH activation	1776	1	292	91% (4000th cycle)	S10
Perilla frutescens	Directly pyrolyzed	655	0.5	270	96% (10000th cycle)	S11
Rice straw	KOH activation	1122	1	337	96% (10000th cycle)	S12
Cotton	KOH activation	1508	1	278	94% (100000th cycle)	S13
Sakura	KOH activation	1434	0.2	266	90% (2000th cycle)	S14
Osmanthus flower	KOH activation	1463	1	255	92% (10000th cycle)	S15
Rugosa rose	KOH activation	1393	0.5	346	96% (10000th cycle)	This work

Table S3 Comparison of maximum monolayer adsorptions of some MB dyes onto various adsorbents in this study and other literatures.

Biomass precursors	S_{BET} (m^2/g)	Q_m (mg/g)	Ref.
Sunflower pith	2090	580.6	S16
Date Press Cake	2633	613.8	S17
Lychee seed	154	124.5	S18
Albizia lebbeck seed pods	1825	381.2	S19
Cotton stalk	729	294.1	S20
Bamboo chip	721	305.3	S21
Karanj fruit hulls	828	239.4	S22
Coconut husk	1356	418.2	S23
Rice husk	752	362.6	S24
Palm shell	895	343.9	S25
Rugosa rose	1393	491.5	This work

Table S4 Correlation coefficient R^2 and constant values of four adsorption kinetics models.

Models	Pseudo-first order	Pseudo-second order	Elovich	Intra-particle
R^2	0.982	0.997	0.946	0.921
Constants	k_1: 0.095 min^{-1}	k_2: 3.37×10^{-5} g/(mg·min)	β: 0.0098 g/(mg·min)	k_{id}: 86.2 g/(mg·$min^{-0.5}$)
	q_e: 387.6 mg/g	q_e: 526.31 mg/g	α: 337.43 g/mg	c: 47.58

Table S5 R^2 and constant values for the different isotherm models.

Models	Langmuir	Freundlich	Temkin	Dubinin-Radushkevich
R^2	0.999	0.847	0.866	0.974
Constants	q_{max}: 505.05 mg/g	1/n: 0.1497	b_t: 46.44 J/mol	B: 7.522×10^{-4} mol^2J^2
	K_L: 0.846 L/g	K_f: 259.83 L/g	a_t: 244.59 L/g	Q_m: 492.7 mg/g

References of supporting materials

[S1] P. Li, C. Yang, D. Yi, S. Li, M. Wang, H. Wang, Y. Jin, W. Wu. Preparation of spherical porous carbon from lignin-derived phenolic resin and its application in supercapacitor electrodes. Int. J. Biol. Macromol. 252(2023), p. 126271

[S2] P. Li, J. Yu, M. Wang,W. Su, C. Yang, B. Jiang, W. Wu. Preparation of symmetrical capacitors from lignin-derived phenol and pani composites with good electrical conductivity. Int. J. Mol. Sci., 24(2023), p. 8661

[S3] P. Li, C. Yang,Y. Wang,W. Su,Y. Wei, W. Wu. Adsorption studies on the removal of anionic and cationic dyes from aqueous solutions using discarded masks and lignin. Molecules, 28(2023), p. 3349

[S4] L.H. Zheng, M.H. Chen, S.X. Liang, Q.F. Lü. Oxygen-rich hierarchical porous carbon derived from biomass waste-kapok flower for supercapacitor electrode. Diam. Relat. Mater., 113 (2021), pp. 108267

[S5] W.H. Qu, Y.Y. Xu, A.H. Lu, X.Q. Zhang, W.C. Li. Converting biowaste corncob residue into high value added porous carbon for supercapacitor electrodes. Bioresour. Technol., 189 (2015), pp. 285-291

[S6] Y.T. Li, Y.T. Pi, L.M. Lu, S.H. Xu, T.Z. Ren. Hierarchical porous active carbon from fallen leaves by synergy of K_2CO_3 and their supercapacitor performance. J. Power Sources, 299 (2015), pp. 519-528

[S7] H.B. Zhao, W.D. Wang, Q.F. Lu, T.T. Lin, Q.L. Lin, H.J. Yang. Preparation and application of porous nitrogen-doped graphene obtained by co-pyrolysis of lignosulfonate and graphene oxide. Bioresour. Technol., 176 (2015), pp. 106-111

[S8] H. Li, D. Yuan, C. Tang, S. Wang, J. Sun, Z. Li, T. Tang, F. Wang, H. Gong, C. He. Lignin-derived interconnected hierarchical porous carbon monolith with large areal/volumetric capacitances for supercapacitor. Carbon, 100 (2016), pp. 151-157

[S9] L. Wan, X. Li, N. Li, M. Xie, C. Du, Y. Zhang, J. Chen. Multi-heteroatom-doped hierarchical porous carbon derived from chestnut shell with superior performance in supercapacitors. J. Alloy. Compd., 790 (2019), pp. 760-771

[S10] L.J. Xie, G.H. Sun, F.Y. Su, X.Q. Guo, Q.Q. Kong, X.M. Li, X.H. Huang, L. Wan, W. Song, K.X. Li, C.X. Lv, C.M. Chen. Hierarchical porous carbon microtubes derived from willow catkins for supercapacitor applications. J. Mater. Chem. A, 4 (2016), pp. 1637-1646

[S11] B. Liu, Y. Liu, H. Chen, M. Yang, H. Li. Oxygen and nitrogen co-doped porous carbon nanosheets derived from Perilla frutescens for high volumetric performance supercapacitors. J. Power Sources, 341 (2017), pp. 309-317

[S12] S. Liu, Y. Zhao, B. Zhang, H. Xia, J. Zhou, W. Xie, H. Li. Nano-micro carbon spheres anchored on porous carbon derived from dual-biomass as high rate performance supercapacitor electrodes. J. Power Sources, 381 (2018), pp. 116-126

[S13] W. Jiang, L. Li, J. Pan, R.A. Senthil, X. Jin, J. Cai, J. Wang, X. Liu. Hollow-tubular porous

carbon derived from cotton with high productivity for enhanced performance supercapacitor. J. Power Sources, 438 (2019), p. 226936

[S14] F. Ma, S.L. Ding, H.J. Ren, Y.H. Liu, Sakura-based activated carbon preparation and its performance in supercapacitor applications. RSC Adv., 9 (2019), pp. 2474-2483

[S15]R. Zou, H.Y. Quan, W.X. Wang, W.M. Gao, Y.H. Dong, D.Z. Chen, Porous carbon with interpenetrating framework from Osmanthus flower as electrode materials for high-performance supercapacitor. Journal of Environmental Chemical Engineering, 6 (2018), pp. 258-265

[S16] M. Baysal, K. Bilge, B. Yılmaz, M. Papila, Y. Yürüm. Preparation of high surface area activated carbon from waste-biomass of sunflower piths: Kinetics and equilibrium studies on the dye removal. Environ. Chem. Eng., 6 (2018), pp. 1702-1713

[S17] Z. Heidarinejad, O. Rahmanian, M. Fazlzadeh, M. Heidari. Enhancement of methylene blue adsorption onto activated carbon prepared from Date Press Cake by low frequency ultrasound. J. Mol. Liq., 264 (2018), pp. 591-599

[S18] S. Sahu, S. Pahi, S. Tripathy, S. K. Singh, A. Behera, U. K. Sahu, R. K. Patel. J. Mol. Liq., 315 (2020), p. 113743.

[S19] M.J. Ahmed, S.K. Theydan. Optimization of microwave preparation conditions for activated carbon from Albizia lebbeck seed pods for methylene blue dye adsorption. Anal. Appl. Pyrol., 105 (2014), pp. 199-208

[S20] H. Deng, G. Li, H. Yang, J. Tang, J. Tang. Preparation of activated carbons from cotton stalk by microwave assisted KOH and K_2CO_3 activation. Chem. Eng. J., 163 (2010), pp. 373-381

[S21] A.H. Jawad, A.S. Abdulhameed. Statistical modeling of methylene blue dye adsorption by high surface area mesoporous activated carbon from bamboo chip using KOH-assisted thermal activation. Energy Ecol. Environ., 5 (2020), pp. 456-469

[S22] M. Danish, T. Ahmad, R. Hashim, N. Said, M.N. Akhtar, J. Mohamad-Saleh, O. Sulaiman. Comparison of surface properties of wood biomass activated carbons and their application against rhodamine B and methylene blue dye. Surf. Interfac., 11 (2018), pp. 1-13

[S23] K.Y. Foo, B.H. Hameed. Coconut husk derived activated carbon via microwave induced activation: effects of activation agents, preparation parameters and adsorption performance. Chem. Eng. J., 184 (2012), pp. 57-65

[S24] K.Y. Foo, B.H. Hameed. Porous structure and adsorptive properties of pineapple peel based activated carbons prepared via microwave assisted KOH and K_2CO_3 activation. Microporous Mesoporous Mater., 148 (2012), pp. 191-195

[S25] K.Y. Foo, B.H. Hameed. Utilization of oil palm biodiesel solid residue as renewable sources for preparation of granular activated carbon by microwave induced KOH activation. Bioresour. Technol., 130 (2013), pp. 696-702